Journal of Applied Polymer Science

Influence of Nanofillers on the Sorption and Diffusion Characteristics of the Solvent in Vulcanized Hydrogenated Nitrile Rubber Nanocomposite

Anusuya Choudhury,[1] Anil K. Bhowmick,[1] Matthias Soddemann[2]

[1]Rubber Technology Centre, Indian Institute of Technology, Kharagpur, Kharagpur 721302, India

[2]Lanxess Deutschland GmbH, 41538 Dormagen, Germany

Correspondence to: A. K. Bhowmick, Indian Institute of Technology, Patna 800013, India (E-mail: anilkb@rtc.iitkgp.ernet.in or E-mail: director@iitp.ac.in)

ABSTRACT: The impact of nanofillers on the swelling characteristics of hydrogenated nitrile butadiene rubber (HNBR)–clay nanocomposites was thoroughly investigated. The nanocomposites exhibited a dramatic decrease in the solvent uptake compared to the unfilled HNBR even at very low filler loadings because of the molecular dispersion of the organically modified montmorillonite and sepiolite and strong interaction between the HNBR and clays. The dispersion of the clay layers was verified by transmission electron microscopy. In addition, the clay content was found to influence the solvent uptake properties of the HNBR–clay nanocomposites. The diffusion and sorption behavior of chloroform in the HNBR–clay nanocomposites at different loadings was studied by a conventional weight gain method. The diffusion results were analyzed in terms of the simple Fickian model. Finally, Arrhenius and thermodynamic parameters were evaluated from these diffusion data. © 2012 Wiley Periodicals, Inc. J. Appl. Polym. Sci. 128: 2556–2562, 2013

KEYWORDS: diffusion; nanocomposites; nanoparticles; nanostructured polymers; nanowires and nanocrystals; rubber

Received 12 July 2011; accepted 16 August 2012; published online 3 November 2012
DOI: 10.1002/app.38475

INTRODUCTION

In the polymer industry, polymer nanocomposites have attracted great attention throughout the scientific world because of their remarkable improvements in material properties (e.g., very high reinforcement, very good barrier properties, improved mechanical behavior, and better flame retardancy) at very low filler loadings (up to 10 wt %) when compared to pristine polymers or conventional composites.[1–14] Nanofillers are of different types, spherical or zero-dimensional nanofillers (e.g., silica nanoparticles), one-dimensional rodlike or fiber-type nanofillers (e.g., synthetic whiskers, carbon nanotubes, sepiolite), two-dimensional sheet or platelet-type nanofillers (e.g., layered silicates such as smectite clays, synthetic mica, and graphite), and three-dimensional nanofillers [e.g., polyhedral oligomeric silsesquioxanes (POSS)].

The most common nanoclay used in the polymer industry is montmorillonite. The model structure consists of two fused silica tetrahedral sheets sandwiching an edge-shared octahedral sheet of either aluminum or magnesium hydroxide. This clay is generally used after organic modification to make it compatible with organic polymers. Sepiolite is another nanoclay, which contains fine microporous channels having dimensions of 0.37 $\times$ 0.16 nm^2 running parallel to the length of the fiber.

Hydrogenated nitrile butadiene rubber (HNBR) has been prepared by the hydrogenation of nitrile rubber in solution with metal catalyst to convert carbon–carbon double bonds into single bond. Because of this conversion, HNBR can replace many industrial polymers because of its good balance of properties, such as its high tensile strength, low permanent set, good abrasion resistance, high elasticity, stability toward thermal aging, and better barrier properties. Thus, HNBR has become a very challenging material in the automotive industry and other specialized applications and was selected for this study.

There have only been a very few studies on HNBR nanocomposites.[15–17] The effect of the curative package shows an interesting effect on the morphology of the nanocomposites. The sulfur vulcanization, in combination with the primary amine intercalants of clay, produces a confined clay structure, whereas peroxide curing yields well-ordered intercalated nanocomposites. Work on HNBR from our laboratory has also been notable.[18,19] Before these investigations, Sadhu and Bhowmick[20,21] discussed the mechanical and dynamic mechanical properties of nitrile rubber nanocomposites. So, the barrier properties of HNBR-based nanocomposites are worth investigating. Extensive work on solvent barrier properties has been documented for

Table I. Sample Name and Designating of the Rubber and Clay

Sample name	Designation	Supplier
Therban C3467	S1	Lanxess, Germany
Cloisite 30B	30B	Southern Clay Products, Gonzales, Texas
Pangel B20	B20	Tolsa S. A, Empres, Mercedes, Spain
DCP	x	Henan Allrich Chemical Co., Ltd. (South America)
Therban C3467 + 1-phr DCP	S1-1x	—
Therban C3467 + 4-phr Closite 30B + 1-phr DCP	S1-30B-4-1x	—
Therban C3467 + 8-phr Closite 30B + 1-phr DCP	S1-30B-8-1x	—
Therban C3467 + 16-phr Closite 30B + 1-phr DCP	S1-30B-16-1x	—
Therban C3467 + 8-phr Pangel B20 + 1-phr DCP	S1-B20-8-1x	—

different rubber–solvent systems.[22–32] However, there have only been a few investigations of solvent barrier properties of nanocomposites.[33–37]

In this study, we focused on the sorption and diffusion of HNBR–clay nanocomposites based on organically modified montmorillonite and sepiolite. These properties have been discussed for different systems in earlier publications.[32,38,39] The transport parameters were calculated for each nanocomposite–solvent system from a conventional weight gain experiment. Furthermore, a study of the temperature dependence of these coefficients was used to calculate the activation parameters and heat of sorption or enthalpy (ΔH).

EXPERIMENTAL

Materials

Therban C3467, having an acrylonitrile content of 34%, a diene content of 5.5%, a Mooney viscosity of 68, and a specific gravity of 0.95, were obtained from Lanxess (Germany). The clay used was Cloisite 30B, purchased from Southern Clay Products (Gonzales, Texas), and Sepiolite Pangel B20, an organophilic sepiolite, which was kindly gifted by Tolsa S. A, Empres (Mercedes, Spain). The specifications were given in earlier publications.[18,19] Details of the different materials used in this investigation are reported in Table I. The solvents used in this study were supplied by Merck, Ltd. (Mumbai, India). The details of the solvents used are shown in Table II.

Table II. Details of Solvents Used in This Study

Sample	Designation	Solubility parameter $[(MPa)^{1/2}]$
Iso-amyl acetate	IAAc	17.20
Chloroform	Ch	18.76
Methyl ethyl ketone	MEK	18.91
Tetrahydrofuran	THF	19.46
Acetone	Ac	20.30
Hydrogenated nitrile butadiene rubber	HNBR	17.90

Preparation of the Rubber–Clay Nanocomposites

The rubber was first dissolved in chloroform (10 w/v % rubber solution). The clay was dispersed in methyl ethyl ketone (MEK) by sonication in an ultrasonicator for 30 min (1 g in 50 mL) at 25°C. A concentration of 1 phr (parts per 100 g of rubber) of dicumyl peroxide (DCP) dispersed in MEK was then added to the rubber solution. The filler dispersion was then poured into the prepared rubber solution, which was finally cast in a Petri dish and dried to get a thin film. The samples were then cured at 150°C for 1 h under 5 MPa of pressure in a hydraulic press to prepare 1 mm thick sheets. The preparation of the nanocomposites by the solution process is shown in Scheme 1. The details of the preparation of the nanocomposites were discussed in our previous publications.[18,19] The designations of the nanocomposite vulcanizates are presented in Table I.

Transmission Electron Microscopy (TEM)

The samples for TEM analysis were prepared by ultracryomicrotomy with a Leica Ultracut (Leica Microsystems GmbH, Vienna, Austria).[18,19] A transmission electron microscope was operated at an accelerating voltage of 200 kV.

Measurement of the Transport Properties

Previously weighed test samples taken for sorption and diffusion experiments were placed into the respective solvent containers (gram of sample vs volume of liquid = 1 : 100). These were then kept in an oven (S. C. Dey & Co., Kolkata, India) to maintain the desired temperature. At periodic intervals, the test samples were removed from the liquid containers, and the extra solvent on the surface was wiped out quickly with blotting

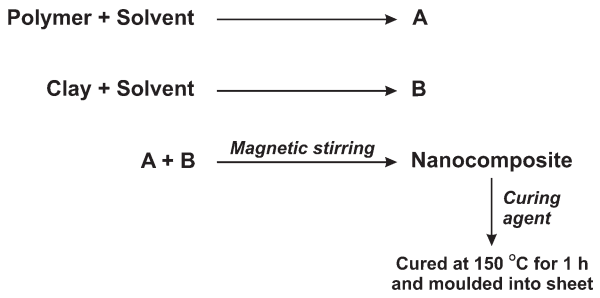

Scheme 1. Preparation of the HNBR–clay nanocomposite vulcanizate.

Applied Polymer SCIENCE

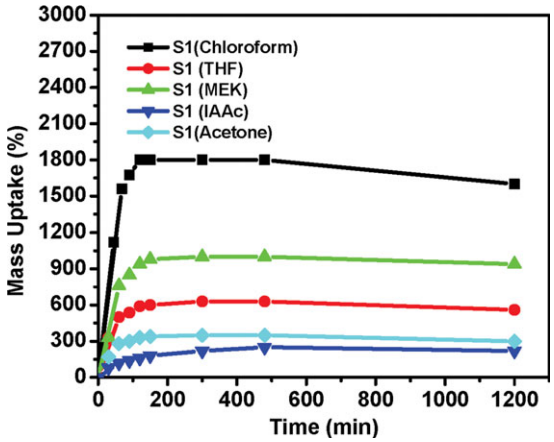

Figure 1. Variation of the percentage mass uptake of unfilled HNBR in different solvents. [Color figure can be viewed in the online issue, which is available at wileyonlinelibrary.com.]

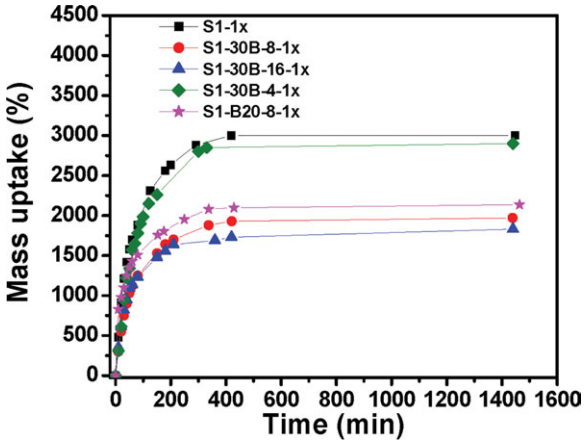

Figure 3. Mass uptake (%) of the unfilled HNBR and its nanocomposites in chloroform. [Color figure can be viewed in the online issue, which is available at wileyonlinelibrary.com.]

paper. Then, the samples were weighed immediately. After weighing, the samples were placed back into the original test bottles. The experiments were performed at 25, 35, and 45°C. The average of three tests is reported here (error limit < 5%).

RESULTS AND DISCUSSION

Swelling Characteristics of the Unfilled HNBR Vulcanizate in Various Solvents

Figure 1 demonstrates the volume swelling characteristics of HNBR vulcanizates in different solvents with time. It is shown in the figure that the swelling reached an optimum value after 150 min for all of the solvents. Although the optimum value of swelling varied for different solvents, the maximum swelling took place in chloroform. Detailed analysis in subsequent sections was done on the results of the chloroform sorption for simplicity.

A plot of the variation of the swelling index of vulcanized HNBR (in different solvents) against the solubility parameter is depicted in Figure 2 (the swelling index is defined as the percentage of volume swelling divided by 100). The swelling index of the vulcanized HNBR matrix increased with the solubility parameter of the solvent and reached its maximum swelling in chloroform and then decreased. The solubility parameter of the cured HNBR was calculated by the group theory method, and the value was 17.90 $MPa^{1/2}$.[34]

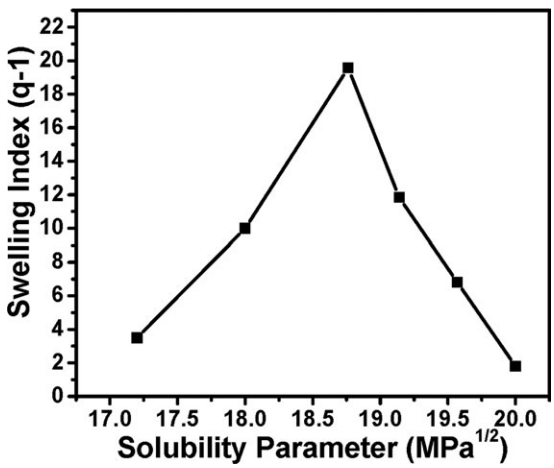

Figure 2. Variation of the swelling index of the unfilled HNBR with the solubility parameter of the solvents.

Influence of the Nanofillers on the Solvent Resistance Behavior of the HNBR Matrix

Figures 3 and 4 demonstrate the solvent uptake behavior of unfilled HNBR and its nanocomposite in chloroform with time. The curves initially proceeded with an almost linear increase and then tended to level off after a certain time interval. Experiments were carried out for longer times to ensure complete equilibrium. The introduction of the nanofillers increased the solvent resistance of the elastomer. Furthermore, with increasing 30B content from 0 to 16 phr, the chloroform uptake of the HNBR nanocomposite decreased from 3000 to 1500% (Figure 3). The dramatic reduction of the solvent uptake in the case of

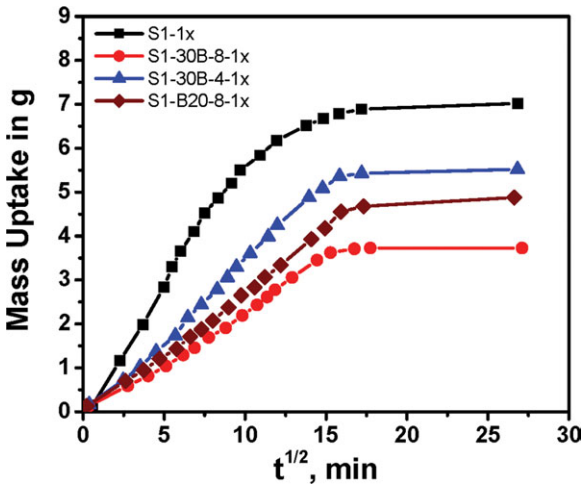

Figure 4. Sorption curve of the unfilled HNBR and nanocomposite at 35°C. The x-axis indicates square root of time in minutes. [Color figure can be viewed in the online issue, which is available at wileyonlinelibrary.com.]

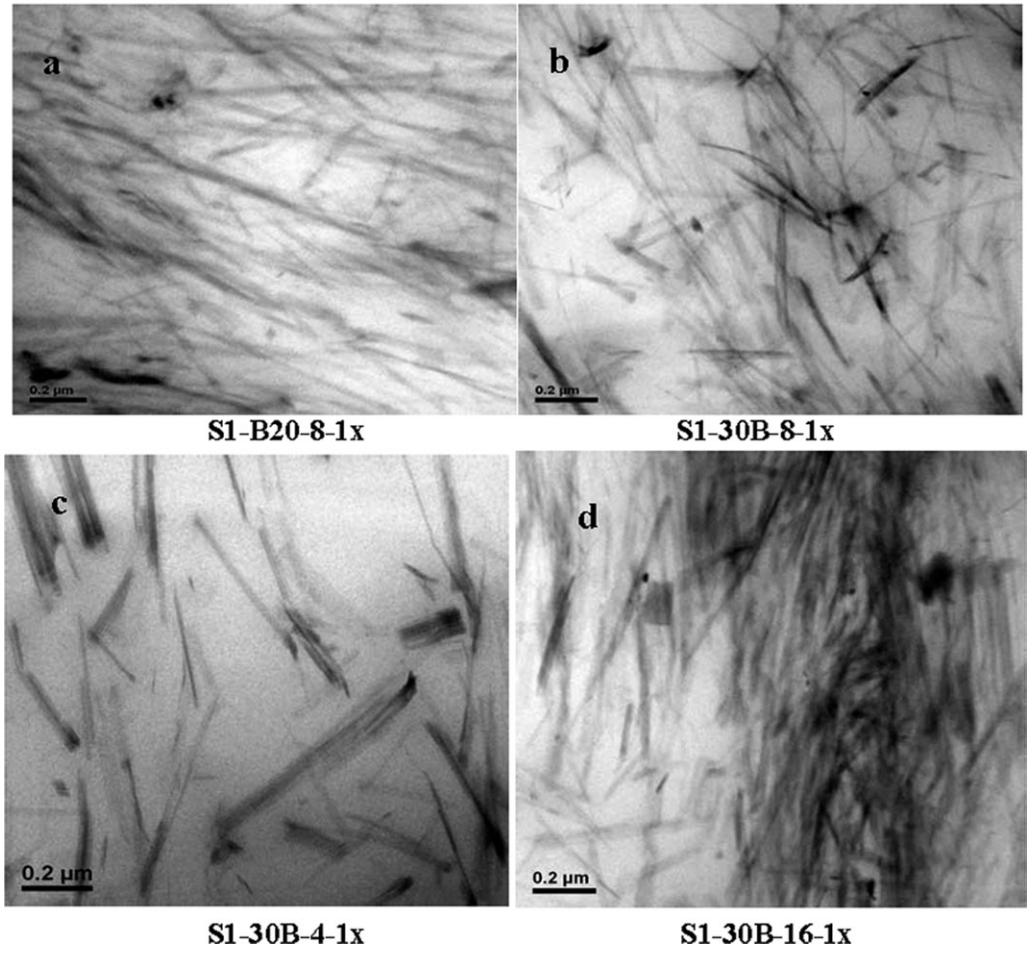

Figure 5. TEM of (a) S1-B20-8-1x, (b) S1-30B-8-1x, (c) S1-30B-4-1x, and (d) S1-30B-16-1x.

the 30B and B20 nanocomposites compared to the virgin HNBR matrix was due to the presence of filler and the good dispersion of these two nanofillers in the HNBR matrix (as confirmed with a TEM photograph and discussed later). The good dispersion of the nanofiller in the matrix increased the surface area of the reinforcing phase, which caused an excellent improvement in the solvent resistance characteristics of the nanocomposite. Moreover, the aspect ratio of the silicate layers present in 30B and the fibrous sepiolite was very large. Also, the strong interaction between the polar HNBR matrix and the OH groups present in the 30B and B20 surface restricted the solvent uptake.[40,41] Thus, the well-dispersed morphology of 30B and B20 were favorable to the solvent barrier properties of the HNBR–filler nanocomposite. The solvent uptake by pure clays was also measured, and we found that both 30B and B20 absorbed a marginal quantity of the solvent (the values were 6 and 3% for 30B and B20, respectively). The nanofillers also formed a mazelike structure, which created an obstacle in the solvent's pathway, and this was also confirmed from the TEM photographs (discussed later). The unfilled S1-1x registered the maximum solvent uptake.

A TEM photograph of S1-B20-8-1x and S1-30B-8-1x is shown in Figure 5(a–b). It is shown in the figure that for the S1-B20-8-1x nanocomposite, rod-shaped fillers were dispersed within the matrix phase [Figure 5(a)]. Figure 5(b) reveals that in the case of S1-30B-8-1x also, the silicate plates were distributed mostly uniformly throughout the matrix. TEM photographs of the S1-30B-4-1x and S1-30B-16-1x nanocomposites are represented in Figure 5(c–d). It is depicted in Figure 5(d) that in the case of S1-30B-16-1x, the filler particles tended to agglomerate because of the presence of a higher filler loading and caused poor dispersion.

Diffusivity

To understand the mechanism of transport of solvent within the matrix, the solvent uptake results were fitted to the following expression:

$$M_t/M_\alpha = Kt^n \quad (1)$$

where n is the rate constant and K is a constant which is a characteristic of the system. When $n = 0.50$, it implies Fickian diffusion. When n is in the range of $0.50 < n < 1.00$, anomalous transport behavior is predicted.[16] M_t is the mass uptake at time t, and M_α is the saturated mass uptake at equilibrium. The plot of mass uptake (M_t/M_α) versus the square root of time of the unfilled elastomer and the representative nanocomposites is shown in Figure 6. M_t is defined as follows:

$$M_t = (W_t - W_0)/W_0 \quad (2)$$

Applied Polymer SCIENCE

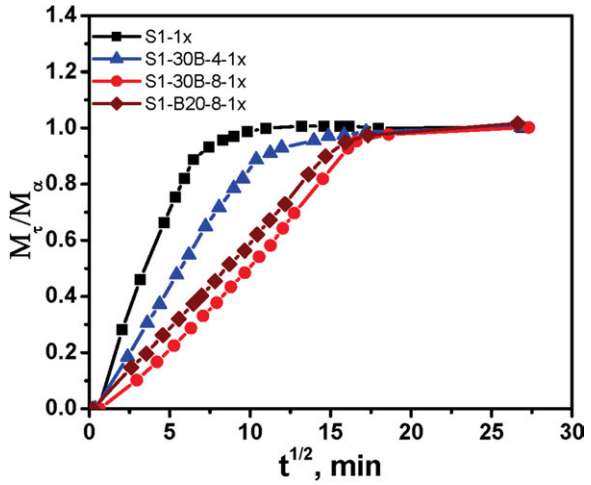

Figure 6. Diffusion curve of HNBR and its nanocomposite. [Color figure can be viewed in the online issue, which is available at wileyonlinelibrary.com.]

where W_t and W_0 are the weight of the sample at time t and the initial weight, respectively. With eq. (1), the n value for different systems was calculated and was found to have a marginal deviation from 0.50. Figure 6 depicts that initially, all of the curves showed almost linear behavior and, thus, followed the simplified Fickian diffusion formula as follows:

$$\frac{M_t}{M_\infty} = 4\left(\frac{Dt}{\Pi l^2}\right)^{\frac{1}{2}} \tag{3}$$

where l is the thickness of the sample.

From the slope of the linear region of the plot (Figure 6), the diffusion coefficient (D) of the solvent molecules into the unfilled elastomer and the nanocomposite was calculated. The results are tabulated in Table III. The highest D value was observed in the case of the unfilled elastomer, S1-1x, and the lowest value was registered for the S1-30B-8-1x nanocomposite; this was followed by S1-30B-16-1x, S1-B20-8-1x, and S1-30B-4-1x. Thus, with the addition of 8-phr 30B, the lowest diffusion of the solvent occurred. In the case of S1-30B-8-1x, the TEM photograph displayed mostly exfoliated particles, along with some intercalated structures and also alignment of the nanofiller layers. From the TEM photograph of S1-30B-16-1x [Figure 5(d)], some agglomeration was observed. In the case of S1-30B-4-1x, on the other hand, the amount of nanofiller per square area was lower, and this was evident from the TEM photograph of the S1-30B-4-1x nanocomposite [Figure 5(c)]. From the TEM photograph, it is shown that the amount of filler available for interaction with the polymer was quite high for the 8-phr loading, and the distribution of filler within the rubber was also good. Thus, the rubber–filler interaction and dispersion were highest for 8 phr of loading [TEM photograph, Figure 5(b)]. Among the two different nanofillers, the 30B nanocomposite registered much lower D than the B20 nanocomposite. In the case of B20, the density of silanol groups on its surface was very high. So, B20 perhaps adsorbed some of the peroxide molecule on its surface. Figure 7(a,b) represents the plot of heat flow versus the temperature of 30B and B20 mixed with peroxide (DCP). It is shown in Figure 7 that in the case of both B20 and 30B, no endothermic or exothermic changes occurred when the experiment was carried out from 50 to 150°C. However, when the nanofillers were heated in the presence of peroxide, a small endothermic peak was observed at about 50°C; this may have been due to the solvent (chloroform) used to mix the clay and curing agent. Furthermore, in the case of the B20 and DCP mix [Figure 7(a)], a small exothermic hump observed at about 130°C, which may have been due to the adsorption of peroxide molecules on the B20 surface was absent for the 30B and DCP mix [Figure 7(b)]. These observations pointed toward the fact that presence of B20 retarded or delayed the peroxide curing reaction. On the other hand, for the S1-30B nanocomposite, an efficient crosslinking took place.

Thermodynamic Interpretation

The solution–diffusion process was the mechanism of permeation of small molecules through the rubbery polymers. The solubility coefficient (S) is defined as the ratio of permeability coefficient (P) to D ($S = P/D$). The apparent S can be expressed in terms of a vant Hoff relationship[16] as follows:

$$\log S = \frac{\Delta S}{2.303R} - \frac{\Delta H}{2.303RT} \tag{4}$$

where R is the universal gas constant and T is the absolute temperature.

With this relationship, ΔH and the entropy (ΔS) of a particular composite–solvent system can be calculated. A plot of log S versus $1/T$ is shown in Figure 8. From the slope of this plot, ΔH could be calculated and ΔS is determined from the intercept. Knowing the values of ΔH and ΔS, the free energy change of the sorption process (ΔG) at 35°C was calculated with the following equation (Table III):

$$\Delta G = \Delta H - T\Delta S \tag{5}$$

We observed that the ΔH values were positive for both the unfilled elastomer and the nanocomposite; this indicated an

Table III. Thermodynamic Parameters for the Nanocomposite–Solvent Systems

Parameter	S1-1x	S1-30B-4-1x	S1-30B-8-1x	S1-30B-16-1x	S1-B20-8-1x
$D \times 10^8$ (cm^2/s)	3.5	1.5	0.4	0.6	0.9
ΔH (kJ/mol)	0.33	—	0.35	—	0.34
ΔS (kJ K^{-1} mol^{-1})	0.31	—	0.25	—	0.29
ΔG (kJ/mol)	−8.56	—	−6.75	—	−7.50
E_D (kJ/mol)	14.78	—	22.17	—	19.20

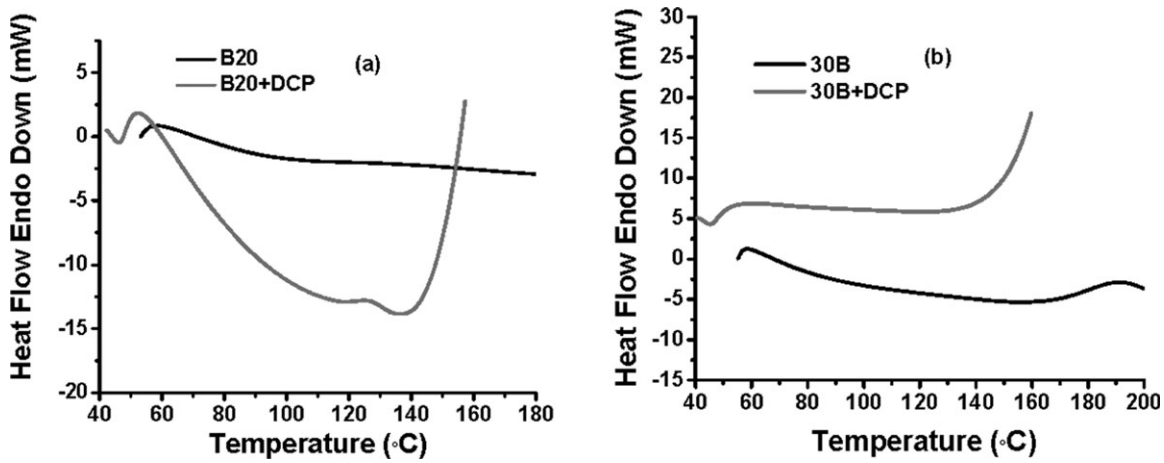

Figure 7. Heat flow versus temperature plots of (a) B20 and DCP mix and (b) 30B and DCP mix.

endothermic process. The ΔG values were negative for both the unfilled elastomer and the nanocomposite; this led to the conclusion that sorption was favorable for all of the systems. However, the ΔG value for the unfilled elastomer was lower (−8.56 kJ/mol) than those of the nanocomposites (−6.75 and −7.50 kJ/mol). This indicated that sorption process became less favorable compared to the unfilled system because of the addition of nanofiller.

The activation energy of diffusion (E_D) could be determined with the following Arrhenius relationship as follows:

$$D = D_0 e\left(\frac{-E_D}{RT}\right) \tag{6}$$

where D_0 is the time independent pre exponential factor.

Figure 9 shows a representative plot of log D versus temperature. The slope of the curves gave the E_D values. The higher E_D value for S1-30B-8-1x (Table III) over the unfilled elastomer was due to the presence of filler and the good dispersion of clay particles into the polymer matrix, as discussed earlier. For S1-B20-8-1x, the E_D value was lower than that of S1-30B-8-1x for the same reason, as discussed earlier. Thus, the addition of nanofillers improved the solvent barrier properties of a polymer because of the combined effect of (1) the good dispersion of the nanofillers in the HNBR matrix, which maximized the available surface area of the reinforcing phase and caused an excellent improvement in the solvent barrier properties of the nanocomposite and (2) the strong interaction between the polar HNBR matrix and the OH groups present in the 30B and B20 surface, which restricted the solvent uptake.

CONCLUSIONS

In this study, the impact of nanofillers on the swelling characteristics of HNBR–clay nanocomposites based on organically modified montmorillonite (30B) and sepiolite was investigated. The introduction of nanofillers led to an obvious decrease in the solvent uptake. Furthermore, as the 30B content increased from 0 to 16 phr, the chloroform uptake of the HNBR–filler nanocomposite decreased from 3000 to 1500%. The dramatic decrease in the solvent uptake in the case of the 30B and B20 nanocomposite compared to the virgin HNBR matrix was due to the good dispersion of the nanofillers in the HNBR matrix

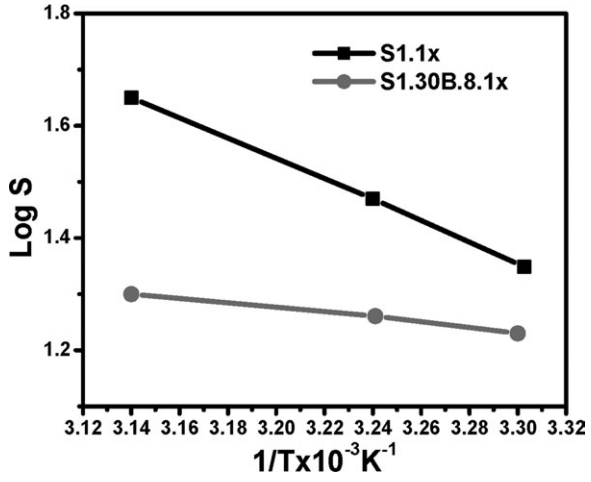

Figure 8. Plot of log S versus the reciprocals of temperature for the unfilled HNBR and nanocomposite.

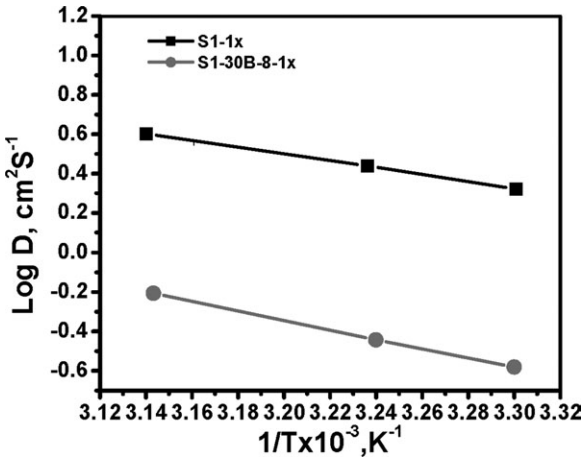

Figure 9. Plot of log D versus temperature for the unfilled HNBR and nanocomposite.

and the strong interaction between the polar HNBR matrix and the OH groups present in the 30B and B20 surface. The solvent diffusion was found to be lowest for S1-30B-8-1x because of the good distribution of filler within the rubber matrix. E_D increased from 14 to 22 kJ/mol with the addition of 8 phr of 30B nanofiller. The results were explained further with the help of thermodynamics. The ΔH values were positive for both the unfilled elastomer and the two nanocomposites; this indicated an endothermic process. The ΔG values were negative, which confirmed that the sorption was favorable for all of the systems. However, the value was lower for the unfilled elastomer (−8.56 kJ/mol) than for the nanocomposites (−6.75 kJ/mol for S1-30B-8-1x and −7.50 kJ/mol for S1-B20-8-1x); this indicated that the sorption was less favorable with the addition of nanoclays compared to the control system.

ACKNOWLEDGMENT

The authors are indebted to Lanxess, Germany for funding the project at Indian Institute of Technology Kharagpur.

REFERENCES

1. Shach, D.; Fytas, G.; Vlassopolelos, D. *Langmuir* **2005**, *21*, 19.
2. Jordan, J. M. *J. Phys. Colloid Chem.* **1950**, *53*, 245.
3. Joley, S. *Chem. Mater.* **2002**, *14*, 4202.
4. Tarapow, J. A.; Bernai, C. R.; Alvarez, V. A. *J. Appl. Polym. Sci.* **2009**, *111*, 768.
5. Maiti, M.; Bhattacharya, M.; Bhowmick, A. K.; *Rubber Chem. Technol.* **2008**, *81*, 384.
6. Koh, H. C.; Park, J. S.; Jeong, M. A.; Hwang, H. Y.; Hong, Y. T.; Ha, S. Y.; Nam, S. Y. *Desalination* **2008**, *233*, 201.
7. Lee, J. H.; Jung, D.; Hong, C. E.; Rhee, K. Y.; Advani, S. G. *Compos. Sci. Technol.* **2005**, *65*, 1996.
8. Wang, S.; Zhang, Y.; Ren, W.; Zhang, Y.; Lin, H. *Polym. Test.* **2005**, *24*, 766.
9. Chaudhary, D. S.; Prasad, R.; Gupta, R. K.; Bhattacharya, S. N. *Thermochim. Acta* **2005**, *433*, 187.
10. Okamoto, M.; Morita, S.; Kotaka, T. *Polymer* **2001**, *42*, 2685.
11. Zhang, J.; Jiang, D. D.; Wilkie, C. A. *Polym. Degrad. Stab.* **2006**, *91*, 358.
12. Liang, Y.; Wang, Y.; Wu, Y.; Lu, Y.; Zhang, H.; Zhang, L. *Polym. Test.* **2005**, *24*, 12.
13. Messermith, P. B.; Giannelis, E. P. *J. Polym. Sci. Part A: Polym. Chem.* **1995**, *33*, 1049.
14. Picard, E.; Vermogen, A.; Gérard, J. F.; Espuche, E. *J. Membr. Sci.* **2007**, *292*, 133.
15. Gatos, K. G.; Szazdi, L.; Pukanszky, B.; Karger-Kocsis, J. *Macromol. Rapid Commun.* **2005**, *26*, 915.
16. Gatos, K. G.; Sawanis, N. S.; Apostolov, A. A.; Thomann, R.; Karger-Kocsis, J. *Macromol. Mater. Eng.* **2004**, *289*, 1079.
17. Herrmann, W.; Uhl, C.; Heinrich, G.; Jehnichen, D. *Polym. Bull.* **2006**, *57*, 395.
18. Choudhury, A.; Ong, C.; Bhowmick, A. K. *Polymer* **2009**, *50*, 201.
19. Choudhury, A.; Ong, C.; Bhowmick, A. K. *J. Appl. Polym. Sci.* **2010**, *116*, 1428.
20. Sadhu, S.; Bhowmick, A. K. *J. Polym. Sci. Part B: Polym. Phys.* **2004**, *42*, 1573.
21. Sadhu, S.; Bhowmick, A. K. *Rubber Chem. Technol.* **2005**, *78*, 321.
22. Cassidy, P. E.; Aminabhavi, T. M. *Rubber Chem. Technol.* **1983**, *56*, 594.
23. Harogoppad, S. B.; Aminabhavi, T. M.; *Macromolecules* **1991**, *24*, 2598.
24. Khinnavar, R. D.; Aminabhavi, T. M. *J. Appl. Polym. Sci.* **1991**, *42*, 2321.
25. Proikakis, C. S.; Mamouzelos, N. J.; Tarantili, P. A.; Andreopoulos, A. G. *Polym. Degrad. Stab.* **2006**, *91*, 614.
26. Gopakumar, S.; Gopinathan Nair, M. R. *Polymer* **2005**, *46*, 10419.
27. Azaar, K.; Rosca, I. D.; Vergnaud, J. M. *Polymer* **2002**, *43*, 4261.
28. Kader, M. A.; Bhowmick, A. K. *Polym. Degrad. Stab.* **2003**, *79*, 283.
29. Mathai, A. E.; Singh, R. P.; Thomas, S. *J. Membr. Sci.* **2002**, *202*, 35.
30. El-Tantawy, F. *Polym. Degrad. Stab.* **2001**, *73*, 289.
31. Erdal, S.; Bahar, I.; Erman, B.; *Polymer* **1998**, *39*, 2035.
32. Sen Majumder, P.; Majali, A. B.; Tikku, V. K.; Bhowmick, A. K. *J. Appl. Polym. Sci.* **2000**, *75*, 784.
33. Brunside, S. D.; Giannelis, E. P. *Chem. Mater.* **1995**, *7*, 1597.
34. Jiang, T.; Wang, Y.; Yeh, J.; Fan, Z. *Eur. Polym. J.* **2005**, *41*, 459.
35. Chen, T.-K; Tien, Y.-I.; Wei, K.-H. *Polymer* **2000**, *41*, 1345.
36. Kim, B. K.; Seo, J. W.; Jeong, H. M. *Eur. Polym. J.* **2003**, *39*, 85.
37. Wang, Z.; Pinnavaia, T. *J. Chem. Mater.* **1998**, *10*, 3769.
38. Alex, R.; Nah, C. *J. Appl. Polym. Sci.* **2006**, *102*, 3277.
39. Valsecchi, R.; Torlaj, L.; Turri, S.; Tonelli, C.; Levi, M. *J. Appl. Polym. Sci.* **2011**, *119*, 3476.
40. Huang, J.-C.; Zhu, Z.-K.; Yin, J.; Qian, X.-F.; Sun, Y.-Y. *Polymer* **2001**, *42*, 873.
41. Kraus, G. J. *J. Appl. Polym. Sci.* **1998**, *8*, 1179.